2

Time-Frequency Transforms

Since its introduction in the early nineteenth century, the Fourier transform has become one of the most widely used signal-analysis tools across many disciplines of science and engineering. The basic idea of the Fourier transform is that any arbitrary signal (of time, for instance) can always be decomposed into a set of sinusoids of different frequencies. The Fourier transform is generated by the process of projecting the signal onto a set of basis functions, each of which is a sinusoid with a unique frequency. The resulting projection values form the Fourier transform (or the frequency spectrum) of the original signal. Its value at a particular frequency is a measure of the similarity of the signal to the sinusoidal basis at that frequency. Therefore, the frequency attributes of the signal can be revealed via the Fourier transform. In many engineering applications, this has proven to be extremely useful in the characterization, interpretation, and identification of signals.

While the Fourier transform is a very useful concept for stationary signals, many signals encountered in real-world situations have frequency contents that change over time. The most common example is music, where the harmonic content of the acoustic signal changes for different notes. In this case, it is not always best to use simple sinusoids as basis functions and characterize a signal by its frequency spectrum. Joint time-frequency transforms were developed for the purpose of characterizing the time-varying frequency content of a signal. The best-known time-frequency representation of a time signal dates back to Gabor [1] and is known as the short-time Fourier transform (STFT). It is basically a moving window Fourier transform. By examining the frequency content of the signal as the time window is

moved, a 2D time-frequency distribution called the spectrogram is generated. The spectrogram contains information on the frequency content of the signal at different time instances. One well-known drawback of the STFT is the resolution limit imposed by the window function. A shorter time window results in better time resolution, but leads to worse frequency resolution, and vice versa. To overcome the resolution limit of the STFT, a wealth of alternative time-frequency representations have been proposed.

In this chapter, we provide an overview of various time-frequency transforms developed by researchers in the signal processing community. They are broadly divided into two classes: linear time-frequency transforms and quadratic (or bilinear) transforms. In Section 2.1, we first discuss linear time-frequency transforms. The discussion commences with the STFT and moves on to two other linear transforms, the continuous wavelet transform (CWT) and the adaptive time-frequency representation. In Section 2.2, we discuss quadratic time-frequency transforms. We begin with the Wigner-Ville distribution (WVD) and discuss Cohen's class and the time-frequency distribution series (TFDS). The main purpose of this chapter is to lay the groundwork for subsequent chapters on radar applications of time-frequency transforms. Emphasis is therefore placed on the application perspective. More detailed theoretical discussions on time-frequency transforms can be found in two excellent texts by Cohen [2] and Qian and Chen [3].

2.1 Linear Time-Frequency Transforms

We begin our discussion of linear time-frequency transforms with a review of the Fourier transform. The Fourier transform of a time signal $s(t)$ is defined as

$$S(\omega) = \int_{-\infty}^{\infty} s(t) \exp\{-j\omega t\} dt \qquad (2.1)$$

where $\omega = 2\pi f$ is the angular frequency. In the context of functional expansion, $S(\omega)$ can be interpreted as the projection of the signal onto a complex exponential function $\exp\{j\omega t\}$ at angular frequency ω. Since the set of exponentials forms an orthogonal basis set, the original function can be constructed from the projection values by the process of

$$s(t) = \frac{1}{2\pi} \int_{-\infty}^{\infty} S(\omega) \exp\{j\omega t\} d\omega \qquad (2.2)$$

which is the inverse Fourier transform of $S(\omega)$. A well-known property of the Fourier transform pair $s(t)$ and $S(\omega)$ is the uncertainty principle. It states that the time duration Δ_t of $s(t)$ and the frequency bandwidth Δ_ω of $S(\omega)$ are related by

$$\Delta_t \Delta_\omega \geq \frac{1}{2} \tag{2.3}$$

where

$$\Delta_t = \left[\frac{\displaystyle\int_{-\infty}^{\infty} (t - \mu_t)^2 |s(t)|^2 \, dt}{\displaystyle\int_{-\infty}^{\infty} |s(t)|^2 \, dt} \right]^{1/2}$$

$$\Delta_\omega = \left[\frac{\displaystyle\int_{-\infty}^{\infty} (\omega - \mu_\omega)^2 |S(\omega)|^2 \, d\omega}{\displaystyle\int_{-\infty}^{\infty} |S(\omega)|^2 \, d\omega} \right]^{1/2}$$

and the mean time μ_t and mean frequency μ_ω are defined as

$$\mu_t = \frac{\displaystyle\int_{-\infty}^{\infty} t |s(t)|^2 \, dt}{\displaystyle\int_{-\infty}^{\infty} |s(t)|^2 \, dt}$$

$$\mu_\omega = \frac{\displaystyle\int_{-\infty}^{\infty} \omega |S(\omega)|^2 \, d\omega}{\displaystyle\int_{-\infty}^{\infty} |S(\omega)|^2 \, d\omega}$$

Thus, the larger the time duration of $s(t)$, the smaller the frequency bandwidth of $S(\omega)$. Conversely, the larger the frequency bandwidth of $S(\omega)$, the shorter the time duration of $s(t)$.

When we use (2.1) to estimate the frequency spectrum of a signal, we assume that the frequency content of the signal is relatively stable during the observation time interval. If the frequency content changes with time, it is not possible to monitor clearly how this variation takes place as a function of time. The reason can be attributed to the nature of the complex sinusoidal basis, which is of infinite duration in time. While the frequency spectrum can still be used to uniquely represent the signal, it does not adequately reflect the actual characteristics of the signal. In the following three subsections, three linear time-frequency transforms (viz., STFT, the CWT, and the adaptive time-frequency representation) are presented. They can be considered as a generalization of the Fourier transform with alternative basis sets that can better reflect the time-varying nature of the signal frequency spectrum.

2.1.1   The STFT

The most standard approach to analyze a signal with time-varying frequency content is to split the time-domain signal into many segments, and then take the Fourier transform of each segment (see Figure 2.1). This is known as the STFT operation and is defined as

$$STFT(t, \omega) = \int s(t')w(t' - t) \exp\{-j\omega t'\}dt' \qquad (2.4)$$

This operation (2.4) differs from the Fourier transform only by the presence of a window function $w(t)$. As the name implies, the STFT is generated by taking the Fourier transform of smaller durations of the original data. Alternatively, we can interpret the STFT as the projection of the function $s(t')$ onto a set of bases $w^*(t' - t) \exp\{j\omega t'\}$ with parameters t and ω. Since the bases are no longer of infinite extent in time, it is possible to monitor how the signal frequency spectrum varies as a function of time. This is accomplished by the translation of the window as a function of time t, resulting in a 2D joint time-frequency representation $STFT(t, \omega)$ of the original time signal. The magnitude display $|STFT(t, \omega)|$ is called the spectrogram of the signal. It shows how the frequency spectrum (i.e., one vertical column of the spectrogram) varies as a function of the horizontal time axis.

Time-domain signal

Short-time Fourier transform
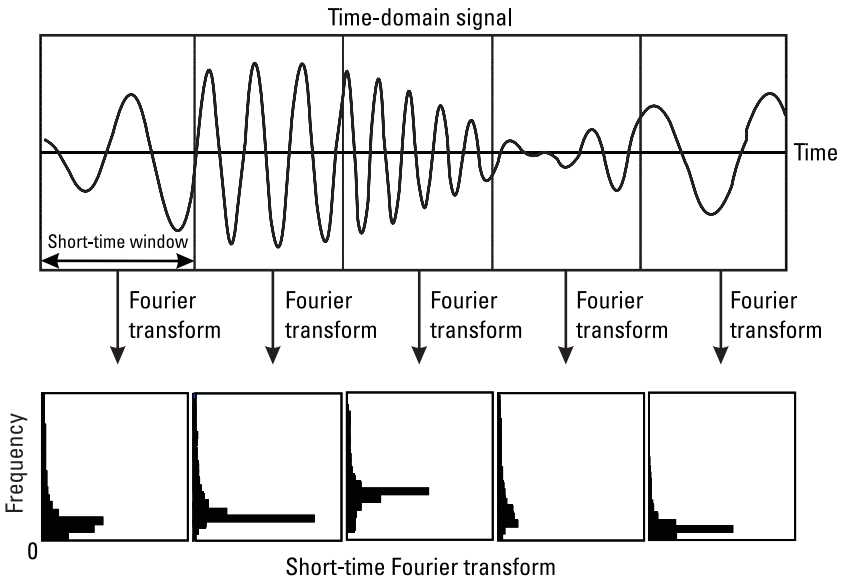
Figure 2.1 Illustration of the STFT.

The definition of the STFT can also be expressed in the frequency domain by manipulating (2.4), with the result

$$STFT(t, \omega) = \frac{1}{2\pi} \exp\{-j\omega t\} \int S(\omega')W(\omega - \omega') \exp\{j\omega' t\}d\omega' \qquad (2.5)$$

Here $W(\omega)$ is the Fourier transform of $w(t)$. The dual relationship between (2.4) and (2.5)[1] is apparent (i.e., the time-frequency representation can be generated via a moving window in time or a moving window in frequency). In addition, we make the following observations: (1) Signal components with durations shorter than the duration of the window will tend to get smeared out [i.e., the resolution in the time domain is limited by the width of the window $w(t)$]. Similarly, the resolution in the frequency domain is limited by the width of the frequency window $W(\omega)$. (2) The window width in time and the window width in frequency are inversely proportional to each other by the uncertainty principle. Therefore, good resolution in time (small time window) necessarily implies poor resolution in frequency (large frequency window). Conversely, good resolution in fre-

---

1. Equation (2.5) has also been referred to as the running-window Fourier transform [4].

quency implies poor resolution in time. (3) The window width in each domain remains fixed as it is translated. This results in a fixed resolution across the entire time-frequency plane. Figure 2.2 shows the basis functions of the STFT and the resulting fixed-resolution cells in the time-frequency plane.

So far, we have not discussed the specific shape of the window function. In general, to cut down on sidelobe interference in the spectrogram, the window function should taper to zero smoothly. Examples of window functions include Hamming, Hanning, Kaiser-Bessel, and Gaussian windows. An STFT using a Gaussian window function is sometimes called the Gabor transform [1]. If we let

$$w(t) = \frac{1}{\pi^{1/4}\sqrt{\sigma}} \exp\left\{-\frac{t^2}{2\sigma^2}\right\} \tag{2.6}$$

the corresponding frequency window is

$$W(\omega) = (2\sigma)^{1/2}\pi^{1/4} \exp\left\{-\frac{\sigma^2\omega^2}{2}\right\} \tag{2.7}$$

From (2.3), we have $\mu_t = 0$, $\mu_\omega = 0$, $\Delta_t = \sigma/\sqrt{2}$, $\Delta_\omega = 1/(\sqrt{2}\sigma)$, and $\Delta_t\Delta_\omega = 1/2$. We can see that the uncertainty equality in (2.3) holds for the
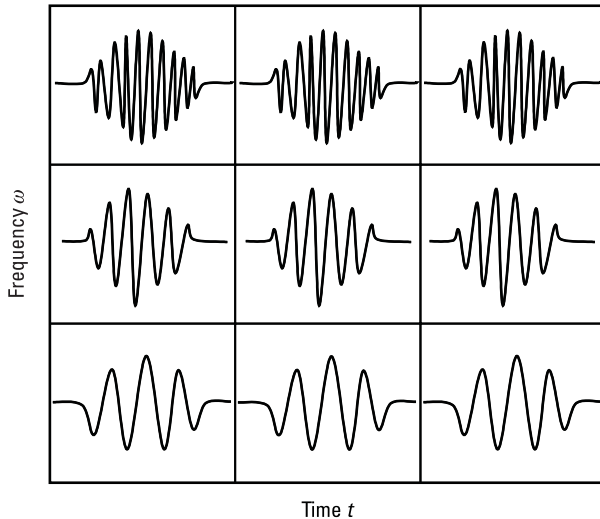
Figure 2.2 Basis functions and the resulting fixed-resolution cells of the STFT.

Gaussian function. Therefore, the Gaussian window function achieves the best time-frequency product among all the possible window functions.

Figure 2.3 shows an example of a signal containing four nonoverlapping, finite-duration sinusoids. Figure 2.3(a) is the time-domain waveform and Figure 2.3(b) shows its corresponding frequency spectrum. Although the four frequencies are well resolved, their time duration information cannot be seen in the frequency domain. Figure 2.3(c) is the STFT spectrogram generated using a Hanning window of 32 points. It shows both the frequency locations and time durations of the four signal components. Figure 2.3(d) is the spectrogram obtained by using a longer time window of 128 points. As expected, a longer time window results in better frequency localization in the time-frequency plane, at the expense of worse time resolution. These results (as well as subsequent examples in this chapter) were generated using the demonstration version of the Joint Time-Frequency Analyzer developed by the National Instruments Corporation [3].
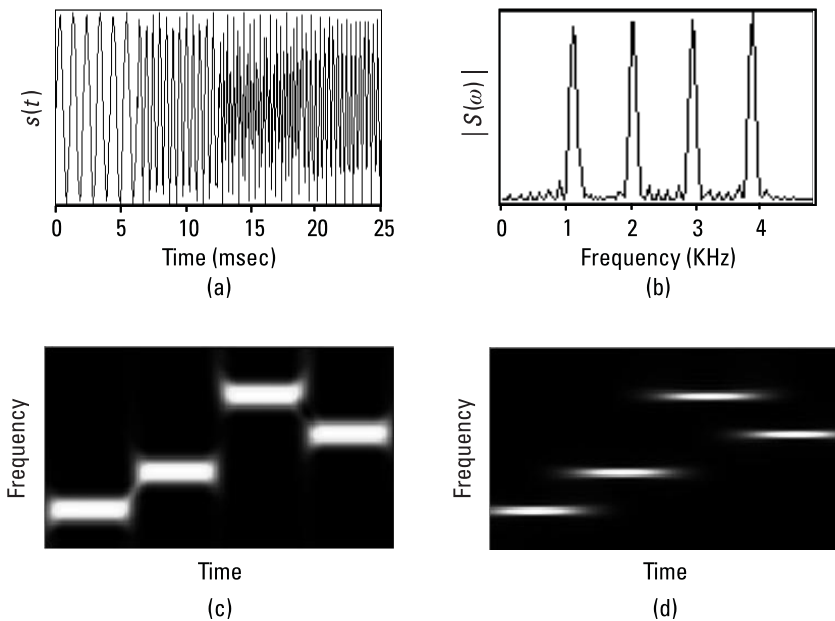
Figure 2.3 (a) A test signal in time consisting of four nonoverlapping, finite-duration sinusoids; (b) its frequency spectrum obtained via the Fourier transform; (c) its spectrogram obtained using STFT with a Hanning window of width 32 points; and (d) its spectrogram with a window of width 128 points. (Plots obtained using the demonstration version of the Joint Time-Frequency Analyzer developed by the National Instruments Corporation [3].)

2.1.2 The CWT

As described in the last section, the spectrogram generated by the STFT is limited in resolution by the extent of the sliding window function. A smaller time window results in better time resolution, but leads to worse frequency resolution, and vice versa. Contrary to the fixed resolution of the STFT, the wavelet transform is a time-frequency representation capable of achieving variable resolution in one domain (either time or frequency) and multiresolution in the other domain [5–8]. The CWT of a signal $s(t)$ can be defined as

$$CWT(t, \omega) = \left(\frac{\omega}{\omega_0}\right)^{1/2} \int s(t') \psi^* \left(\frac{\omega}{\omega_0}(t' - t)\right) dt' \qquad (2.8)$$

$\psi(\cdot)$ is usually termed the "mother wavelet" in wavelet theory. The ratio (ω_0/ω) is the scale parameter and the resulting 2D magnitude display of the above expression is called the scalogram. Let us assume that the mother wavelet is centered at time zero and oscillates at frequency ω_0. Essentially, (2.8) can be interpreted as a decomposition of the signal $s(t')$ into a family of shifted and dilated wavelets $\psi[(\omega/\omega_0)(t' - t)]$. The wavelet basis function $\psi[(\omega/\omega_0)(t' - t)]$ has variable width according to ω at each time t. The $\psi[(\omega/\omega_0)(t' - t)]$ is wide for small ω and narrow for large ω. By shifting $\psi(t')$ at a fixed parameter ω, the (ω_0/ω)-scale mechanisms in the time response $s(t')$ can be extracted and localized. Alternatively, by dilating $\psi(t')$ at a fixed t, all of the multiscale events of $s(t')$ at t can be analyzed according to the scale parameter (ω_0/ω). This is the multiresolution property of the wavelet transform and is an advantage over the STFT for analyzing multiscale signals.

The wavelet transform can also be carried out on the inverse Fourier transform $S(\omega)$ of the signal $s(t)$

$$CWT(t, \omega) = \frac{(\omega_0/\omega)^{1/2}}{2\pi} \int S(\omega') \Psi^* \left(\frac{\omega_0}{\omega}\omega'\right) \exp\{j\omega't\} d\omega' \quad (2.9)$$

where $\Psi(\omega')$ is the Fourier transform of $\psi(t')$. Notice that (2.9) is essentially the Fourier transform of $S(\omega')\Psi^*[(\omega_0/\omega)\omega']$. By comparing (2.9) and (2.5), we observe that $\Psi^*(\omega')$ is similar to the frequency window function $W(\omega')$ in the running window Fourier transform. However, $\Psi(\omega')$ must satisfy the "admissibility condition" in wavelet theory, namely, $\Psi(0) = 0$,

(i.e., it contains no dc components). To satisfy this condition, $\Psi(\omega')$ can be thought of as a shifted window function with a center frequency of ω_0. By changing ω, $\Psi[(\omega_0/\omega)\omega']$ is shifted to ω' and the width of the window is dilated by the factor (ω/ω_0). The ratio between the window width and the window center (or the Q-factor of the window function) remains fixed for all ω values. This is the constant-Q property of the wavelet filter and is in contrast to the STFT where the window width does not change as it is being shifted.

Figure 2.4 illustrates the basis functions in the CWT and the resulting time-frequency grid. Note that both the CWT and the STFT can be interpreted as the decomposition of the time signal $s(t)$ into a family of basis functions that determine the properties of the transform. The STFT and the CWT are similar to each other in that they both use finite basis functions. This is in contrast to the Fourier transform, which uses bases of infinite extent. As is shown in Figure 2.4, however, the width of the basis function in the CWT changes according to the frequency parameter, leading to variable resolution of the time-frequency plane.

2.1.3 Adaptive Time-Frequency Representation

Wavelet use is a step toward variable resolution in the time-frequency plane. However, it is still rather rigid in its particular form of the time-frequency
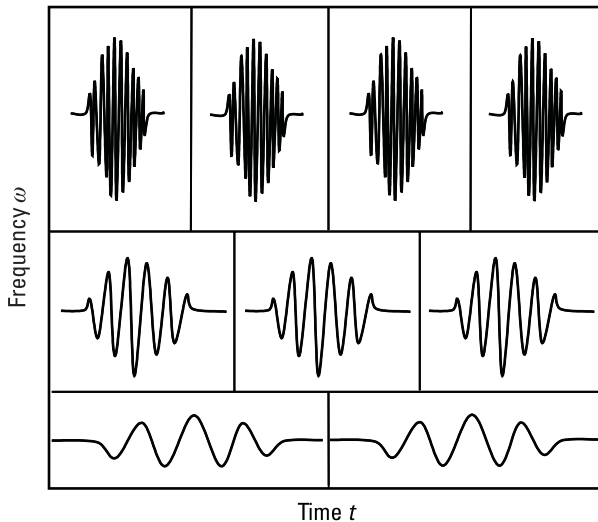
Figure 2.4 Basis functions and the resulting variable-resolution cells of the CWT.

grid. More flexible resolution in the time-frequency plane to accommodate components of the signal with different resolutions is sometimes desirable. Several signal-adaptive time-frequency representations have been proposed in the literature for this purpose, the best known of which are the adaptive Gaussian representation [9] and the matching pursuit algorithm [10]. The adaptive spectrogram (ADS), which we will discuss here, uses adaptive normalized Gaussian functions to represent the signal. In the algorithm, the time and frequency resolutions, as well as the time-frequency centers, are adjusted to best match the signal. The objective of this method is to expand a signal $s(t)$ in terms of normalized Gaussian functions $h_p(t)$ with an adjustable standard deviation σ_p and a time-frequency center (t_p, ω_p) as follows:

$$s(t) = \sum_{p=1}^{\infty} B_p h_p(t) \tag{2.10}$$

where

$$h_p(t) = (\pi\sigma_p^2)^{-1/4} \exp\left\{ -\frac{(t - t_p)^2}{2\sigma_p^2} \right\} \exp\{j\omega_p t\} \tag{2.11}$$

Note that the modulated Gaussian basis has a dual form in its Fourier transform representation

$$H_p(\omega) = (\pi(1/2\pi\sigma_p)^2)^{-1/4} \exp\left\{ -\frac{(\omega - \omega_p)^2}{2(1/\sigma_p)^2} \right\} \exp\{-j(\omega - \omega_p)t_p\} \tag{2.12}$$

Therefore, these basis functions have a time-frequency extent given by σ_p and $(1/\sigma_p)$, respectively (see Figure 2.5).

The coefficients B_p are found one at a time by an iterative procedure. We begin at the stage $p = 1$ and choose the parameters σ_p, t_p, and ω_p such that $h_p(t)$ is the basis with the maximum projection onto the signal

$$B_p = \max_{\sigma_p, t_p, \omega_p} \int s_{p-1}(t) h_p^*(t) dt \tag{2.13}$$

where $s_0(t) = s(t)$. For $p > 1$, $s_p(t)$ is the remainder after the orthogonal projection of $s_{p-1}(t)$ onto $h_p(t)$ has been removed from the signal
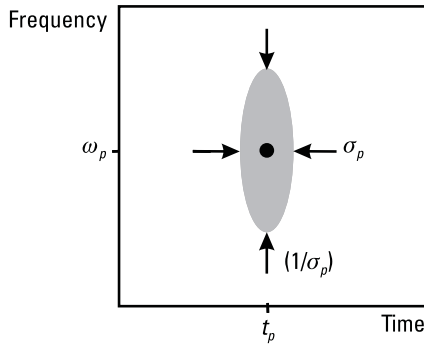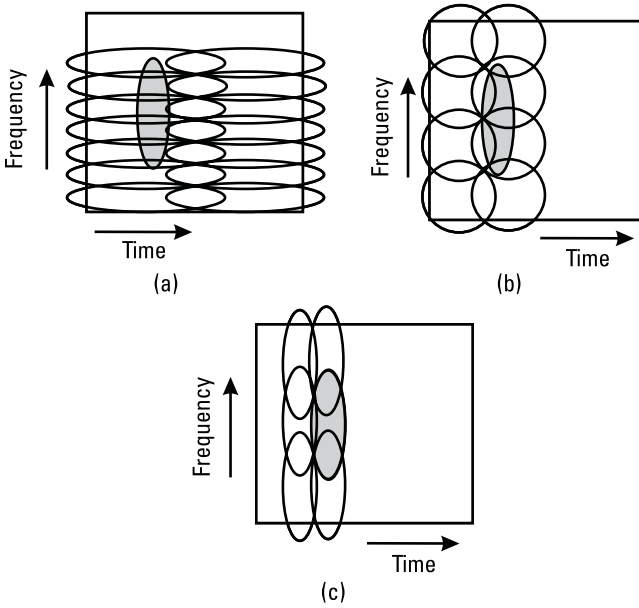
Figure 2.5 Time-frequency representation of a modulated Gaussian basis function centered at (t_p, ω_p) with standard deviation σ_p. (*Source:* [11] © 1997 IEEE.)

$$s_p(t) = s_{p-1}(t) - B_p(t)h_p(t) \tag{2.14}$$

This procedure is iterated to generate as many coefficients as needed to accurately represent the original signal.

Several comments can be made about the adaptive Gaussian representation. First, it can be shown that the norm of the residue monotonically decreases and converges to zero. Therefore adding a new term in the series does not affect the previously selected parameters. Second, because this representation is adaptive, it will generally be concentrated in a very small subspace. As a result, we can use a finite summation of the terms in (2.10) to approximate the signal with a small residual error. Also, since random noise is in general distributed uniformly in the entire time-frequency space, this subspace representation actually increases the signal-to-noise ratio. (Chapter 3 discusses the denoising issue in detail.) Finally, the major difficulty in implementing this algorithm is the determination of the optimal elementary function at each stage. One implementation strategy is to start with a large σ_p and scan the data in frequency and time for a peak. We then divide σ_p by two and find the new peak. This procedure is continued until the standard deviation is small enough (as shown in Figure 2.6). We then select the highest peak and extract the residual using (2.14). It should be pointed out that the fast Fourier transform can be used during this search procedure to obtain the coefficients for all the frequency centers at once, speeding up a search that would otherwise be very time consuming.

The result of applying the adaptive Gaussian extraction can be effectively displayed in the time-frequency plane using the so-called ADS:

Figure 2.6 Illustration of the search strategy for the adaptive Gaussian representation: (1) start with large σ basis and locate the time-frequency position of the peak; (2) divide σ and the search region by two and repeat the search; and (3) repeat this procedure until the highest peak is found. (*Source:* [11] © 1997 IEEE.)

$$ADS(t, \omega) = 2\sum_p |B_p|^2 \exp\left[-\frac{(t - t_p)^2}{\sigma_p^2} - \sigma_p^2(\omega - \omega_p)^2\right] \quad (2.15)$$

This representation is obtained by calculating the WVD (to be discussed in Section 2.2.1) of (2.10) and then deleting the cross terms. It can be shown that the energy contained in the ADS is identical to the energy contained in the signal. Therefore it can be considered as a signal energy distribution in the time-frequency domain. It is also nonnegative, free of cross-term interference, and of high resolution. Figure 2.7 shows the ADS of the test signal shown in Figure 2.3(a).

Further extension of the Gaussian basis functions to include other higher-order phase terms such as chirps have also been reported in [12, 13].

2.2 Bilinear Time-Frequency Transforms

The power spectrum of a signal $s(t)$ is the magnitude square of its Fourier transform, $|S(\omega)|^2$. It can also be expressed as the Fourier transform of the autocorrelation function of $s(t)$
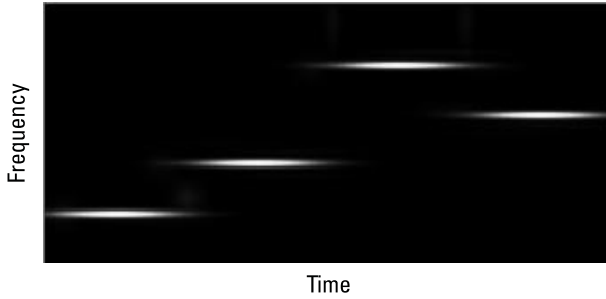
Figure 2.7 The ADS of the test signal with four nonoverlapping, finite-duration sinusoids.

$$|S(\omega)|^2 = \int R(t')e^{-j\omega t'}dt' \tag{2.16}$$

where the autocorrelation function is given by

$$R(t') = \int s(t)s^*(t - t')dt \tag{2.17}$$

The power spectrum indicates how the signal energy is distributed in the frequency domain. While the Fourier transform $S(\omega)$ is a linear function of $s(t)$, the power spectrum is a quadratic function of $s(t)$. Therefore, time-frequency distributions derived directly from the Fourier transform, such as those discussed in Section 2.1, can be classified as linear transforms, while it is customary to call those distributions derived from the power spectrum quadratic (or bilinear) time-frequency distributions. The main impetus for quadratic time-frequency distribution is to define an appropriate time-dependent power spectrum. In this section, we shall discuss three such time-frequency transforms, the WVD, Cohen's class, and the TFDS.

2.2.1 The WVD

The most basic of the quadratic time-frequency representations, the WVD, was first developed in quantum mechanics by Wigner in 1932 [14] and later introduced for signal analysis by Ville [15]. In the WVD, a time-dependent autocorrelation function is chosen as

$$R(t, t') = s\left(t + \frac{t'}{2}\right)s^*\left(t - \frac{t'}{2}\right) \tag{2.18}$$

The WVD of $s(t)$ is then defined as the Fourier transform of this time-dependent autocorrelation function

$$WVD(t, \omega) = \int s\left(t + \frac{t'}{2}\right) s^*\left(t - \frac{t'}{2}\right) \exp\{-j\omega t'\} dt' \qquad (2.19)$$

The WVD can also be defined based on the Fourier transform of $s(t)$ as follows:

$$WVD(t, \omega) = \frac{1}{2\pi} \int S\left(\omega + \frac{\omega'}{2}\right) S^*\left(\omega - \frac{\omega'}{2}\right) \exp\{j\omega' t\} d\omega'$$
$$(2.20)$$

The WVD has a number of desirable properties that make it a good indicator of how the energy of the signal can be viewed as a function of time and frequency. First the WVD of any signal is always real. Second, it satisfies the *time marginal condition*

$$\frac{1}{2\pi} \int WVD(t, \omega) d\omega = |s(t)|^2 \qquad (2.21)$$

That is, by summing the time-frequency distribution over all frequencies, we obtain the instantaneous energy of the signal at a particular time instance. Similarly, the WVD also satisfies the *frequency marginal condition* given by

$$\int WVD(t, \omega) dt = |S(\omega)|^2 \qquad (2.22)$$

In this case, by summing the time-frequency distribution over all time, we obtain the power spectrum of the signal at a particular frequency. Third, the WVD satisfies the *instantaneous frequency property*. If $s(t) = A(t) \exp\{j\alpha(t)\}$, then the average frequency for a given time t is

$$\mu_{\omega/t} = \frac{\int \omega\, WVD(t, \omega) d\omega}{\int WVD(t, \omega) d\omega} = \frac{d}{dt}\alpha(t) \qquad (2.23)$$

That is, the mean frequency computed from the WVD is equal to the derivative of the phase (i.e., the mean instantaneous frequency of the signal). Similarly, the WVD also satisfies the *group delay property*. If $S(\omega) = B(\omega) \exp\{j\beta(\omega)\}$, then the group delay for a given ω is

$$\mu_{t/\omega} = \frac{\int t\, WVD(t, \omega)\, dt}{\int WVD(t, \omega)\, dt} = -2\pi \frac{d}{d\omega}\beta(\omega) \tag{2.24}$$

It implies that the mean time computed from the WVD is equal to the derivative of the spectral phase (i.e., the group delay of the signal).

Although the WVD has many nice properties and gives nearly the best resolution among all the time-frequency techniques, its main drawback comes from cross-term interference. Simply put, the WVD of the sum of two signals is not the sum of their WVDs. If $s = s_1 + s_2$, it can be shown that

$$WVD_s(t, \omega) = WVD_{s_1}(t, \omega) + WVD_{s_2}(t, \omega) + 2\mathrm{Re}\{WVD_{s_1 s_2}(t, \omega)\} \tag{2.25}$$

where the last term is the cross WVD of s_1 and s_2 given by

$$WVD_{s_1 s_2}(t, \omega) = \int s_1\left(t + \frac{t'}{2}\right) s_2^*\left(t - \frac{t'}{2}\right) \exp\{-j\omega t'\}\, dt' \tag{2.26}$$

As a result, if a signal contains more than one component in the joint time-frequency plane, its WVD will contain cross terms that occur halfway between each pair of autoterms. The magnitude of these oscillatory cross terms can be twice as large as the autoterms and yet they do not possess any physical meaning. Figure 2.8 shows an example of a signal containing four finite-duration sinusoids shown earlier in Figure 2.3(a). We can see that even though the WVD has very good time-frequency localization, there are cross-term interference terms between every pair of signal components. This drawback severely hinders the usefulness of the WVD for detecting signal characteristics in the time-frequency plane.

2.2.2 Cohen's Class

In addition to the WVD, a number of bilinear distributions have also been proposed by researchers for time-frequency signal analysis [16–18]. In 1966,
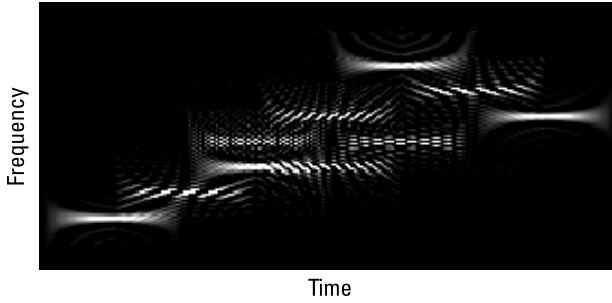
Figure 2.8 The WVD of the test signal with four nonoverlapping, finite-duration sinusoids.

Cohen showed that all these existing time-frequency distributions could be written in a generalized form [19]. Moreover, this general form can be used to facilitate the design of new time-frequency transforms. This class of transforms is now known simply as Cohen's class. We shall describe the general form of Cohen's class, followed by two well-known members of the class for reducing the cross-term interference problem in the WVD.

The general form of Cohen's class is defined as

$$C(t, \omega) = \int\int s\left(u + \frac{t'}{2}\right)s^*\left(u - \frac{t'}{2}\right)\phi(t - u, t')\exp\{-j\omega t'\}dudt' \tag{2.27}$$

The Fourier transform of $\phi(t, t')$, denoted as $\Phi(\theta, t')$, is called the kernel function. It can easily be seen that if $\Phi(\theta, t') = 1$, then $\phi(t, t') = \delta(t)$ and (2.27) reduces to the WVD defined in (2.19). Therefore, the WVD is a member of Cohen's class. More generally, other types of kernel functions can be designed to reduce the cross-term interference problem of the WVD. Two such time-frequency distributions are the Choi-Williams distribution (CWD) and the cone-shaped distribution (CSD).

The CWD [20] uses as its kernel function

$$\Phi(\theta, t') = \exp\{-\alpha(\theta t')^2\} \tag{2.28}$$

Along the θ-axis and the t'-axis, the kernel function is identically one while away from the two axes, the function decays with the damping controlled by α. The inverse Fourier transform of $\Phi(\theta, t')$ is given by

$$\phi(t, t') = \frac{1}{\sqrt{4\pi\alpha(t')^2}} \exp\left\{-\frac{t^2}{4\alpha(t')^2}\right\} \qquad (2.29)$$

and the CWD is defined as

$$CWD(t, \omega) = \int\int \frac{1}{\sqrt{4\pi\alpha(t')^2}} \qquad (2.30)$$

$$\exp\left\{-\frac{(t-u)^2}{4\alpha(t')^2}\right\} s\left(u + \frac{t'}{2}\right) s^*\left(u - \frac{t'}{2}\right) \exp\{-j\omega t'\} du dt'$$

Note that the kernel function is essentially a low-pass filter in the θ-t' plane. It preserves all cross terms that are on the θ-axis and t'-axis. As a result, the CWD usually contains strong horizontal and vertical cross terms in the time-frequency plane. Figure 2.9 shows the CWD of the same test signal containing four finite-duration sinusoids. It preserves the property of the WVD while reducing cross-term interference.

The CSD was introduced by Zhao, Atlas, and Marks [21]. Its name comes from the definition of a cone-shaped $\phi(t, t')$

$$\phi(t, t') = \begin{cases} g(t'), & |t'| \geq 2|t| \\ 0 & otherwise \end{cases} \qquad (2.31)$$

which is confined to the region bounded by lines $t' = 2t$ and $t' = -2t$. In this case, the corresponding kernel function is of the form

$$\Phi(\theta, t') = g(t')|t'|\, \text{sinc}\left(\frac{\theta t'}{2}\right) \qquad (2.32)$$
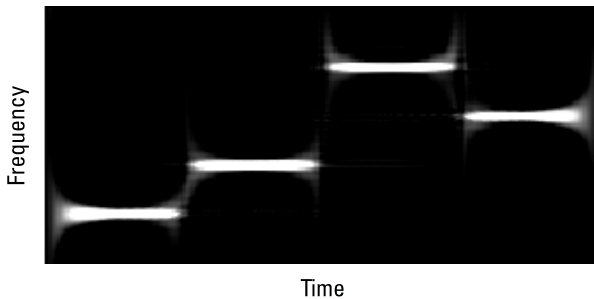
Figure 2.9 The CWD of the test signal with four nonoverlapping, finite-duration sinusoids.

For example, if we choose $g(t') = (1/|t'|) \exp\{-\alpha(t')^2\}$, then the kernel function is $\Phi(\theta, t') = \exp\{-\alpha(t')^2\} \operatorname{sinc}(\theta t'/2)$. In this case, the kernel function is one along the θ-axis and $\exp\{-\alpha(t')^2\}$ along the t'-axis where α controls the decay. Figure 2.10 shows the CSD of the same test signal. Again, the CSD reduces cross-term interference while nearly maintaining the resolution of the WVD.

2.2.3   The TFDS

Another approach to overcoming the cross-term interference problem of the WVD is the TFDS, proposed by Qian and Chen [22]. They suggested that if the WVD can be decomposed into a sum of localized and symmetric functions, it may be possible to suppress cross-term interference by selecting only the low-order harmonics. This is accomplished by first decomposing the original signal into the Gabor expansion

$$s(t) = \sum_m \sum_n C_{m,n} h_{m,n}(t) \qquad (2.33)$$

where

$$h_{m,n}(t) = (\pi\sigma^2)^{-1/4} \exp\left\{\frac{(t - m\Delta t)^2}{2\sigma^2} + jn\Delta\omega t\right\} \qquad (2.34)$$

are time-shifted and frequency-modulated Gaussian basis functions. In the above expression, m and Δt are respectively the time sampling index and time sampling interval, while n and $\Delta\omega$ are the sampling index and sampling interval in frequency. In other words, C_{mn} represents the STFT of the function $s(t)$ using a Gaussian window and evaluated on a sampled grid.
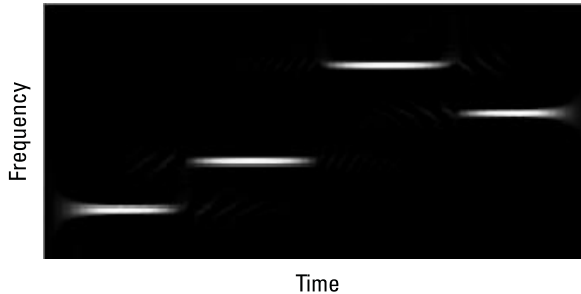
Figure 2.10 The CSD of the test signal with four nonoverlapping, finite-duration sinusoids.

By taking the WVD of both sides of (2.33), we obtain

$$WVD(t, \omega) = \sum_{mn} \sum_{m'n'} C_{m,n} C^*_{m',n'} WVD_{h,h'}(t, \omega) \qquad (2.35)$$

where $WVD_{h,h'}$ denotes the WVD between any pair of basis functions and is available in closed form. Next, the above expression can be regrouped based on the "interaction distance"

$$D = |m - m'| + |n - n'| \qquad (2.36)$$

between the pairs of bases (m, n) and (m', n'). This results in what is termed the TFDS, also called the Gabor spectrogram:

$$
\begin{aligned}
TFDS_D(t, \omega) = &\sum_{mn} |C_{m,n}|^2 WVD_{h,h'}(t, \omega) & (D = 0 \text{ terms}) \\
&+ \sum_{mn} \sum_{m'n'} C_{m,n} C^*_{m',n'} WVD_{h,h'}(t, \omega) & (D = 1 \text{ terms}) \\
&+ \sum_{mn} \sum_{m'n'} C_{m,n} C^*_{m',n'} WVD_{h,h'}(t, \omega) & (D = 2 \text{ terms}) \\
&+ \ldots & (2.37)
\end{aligned}
$$

Clearly, if we take all the terms in the series ($D = \infty$), the right-hand side of (2.37) converges to the WVD of the original signal. This yields the best resolution but is plagued by cross-term interference. At the other extreme, if we take only the self-interaction terms in the series ($D = 0$), the resulting right-hand side is equivalent to the spectrogram of the signal using a Gaussian window function. It has no cross-term interference problem but has the worst resolution. As the order D increases, we gain in resolution but pay a price in cross-term interference. It is often possible to balance the resolution against cross-term interference by adjusting the order D. The optimal value for D was reported to be around 2 to 4.

Figure 2.11 shows the effect of the order D on the frequency-hopping signal discussed in earlier examples. For $D = 0$ [Figure 2.11(a)] the signal has the least time-frequency resolution, but is devoid of cross-term effects. Figure 2.11(b, c) show respectively the TFDS for $D = 3$ and $D = 6$. We see that at $D = 3$ it is possible to capture the most useful information in the time-frequency plane without the degrading effect of the cross terms.
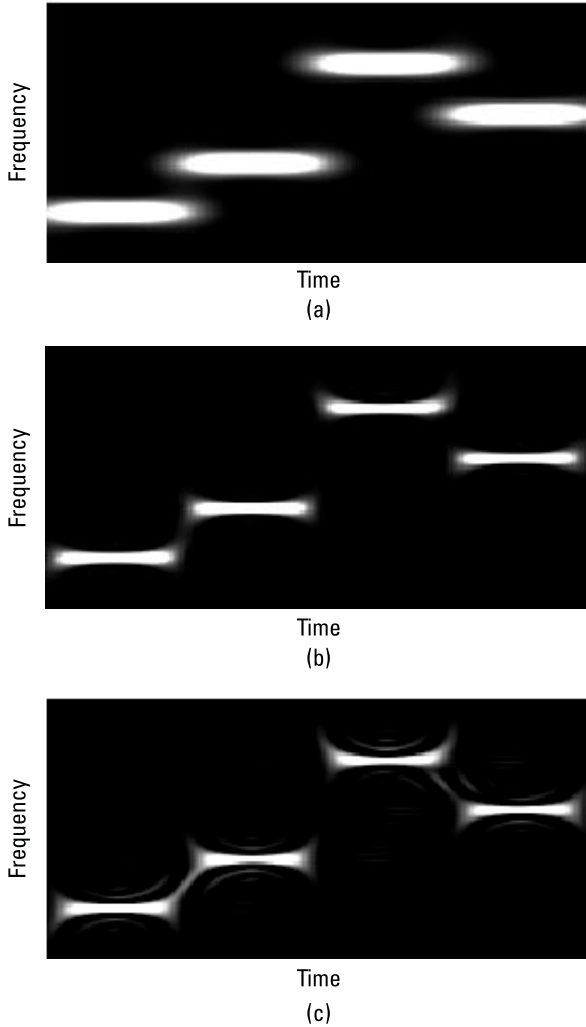
Figure 2.11 The TFDS of the test signal with four nonoverlapping, finite-duration sinusoids: (a) $D = 0$; (b) $D = 3$; and (c) $D = 6$.

In summary, we have described a number of popular time-frequency distributions in this chapter. The list includes the STFT, the CWT, the adaptive joint time-frequency representation, the WVD, Cohen's class, and the TFDS. These time-frequency transforms will be used in subsequent chapters of this book for various applications of radar imaging and signal analysis.

References

[1] Gabor, D., "Theory of Communication," *J. IEE (London)*, Vol. 93, No. III, November 1946, pp. 429–457.

[2] Cohen, L., *Time-Frequency Analysis*, Englewood Cliffs, NJ: Prentice Hall, 1995.

[3] Qian, S., and D. Chen, *Introduction to Joint Time-Frequency Analysis—Methods and Applications*, Englewood Cliffs, NJ: Prentice Hall, 1996.

[4] Moghaddar, A., and E. K. Walton, "Time-Frequency-Distribution Analysis of Scattering from Waveguide Cavities," *IEEE Trans. Antennas Propagat.*, Vol. AP-41, pp. 677–680, May 1993.

[5] Goupillaud, P., A. Grossman, and J. Morlet, "Cycle-Octave and Related Transforms in Seismic Signal Analysis," *Geoexploration*, Vol. 23, 1984, pp. 85–102.

[6] Heil, C. E., and D. F. Walnut, "Continuous and Discrete Wavelet Transforms," *SIAM Review*, Vol. 31, December 1989, pp. 628–666.

[7] Daubechies, I., "The Wavelet Transform, Time-Frequency Localization and Signal Analysis," *IEEE Trans. Inform. Theory*, Vol. IT-36, September 1990, pp. 961–1005.

[8] Combes, J. M., A. Grossmann, and P. Tchamitchian (eds.), *Wavelets, Time-Frequency Methods and Phase Spaces*, Berlin: Springer-Verlag, 1989.

[9] Qian, S., and D. Chen, "Signal Representation Using Adaptive Normalized Gaussian Functions," *Signal Processing*, Vol. 36, March 1994, pp. 1–11.

[10] Mallat, S. G., and Z. Zhang, "Matching Pursuits with Time-Frequency Dictionaries," *IEEE Trans. Signal Processing*, Vol. SP-41, December 1993, pp. 3397–3415.

[11] Trintinalia, L. C., and H. Ling, "Joint Time-Frequency ISAR Using Adaptive Processing," *IEEE Trans. Antennas Propagat.*, Vol. AP-45, February 1997, pp. 221–227.

[12] Qian, S., D. Chen, and Q. Yin, "Adaptive Chirplet Based Signal Approximation," *Proc. ICASSP*, Vol. III, May 1998, pp. 1871–1874.

[13] Bultan, A., "A Four-Parameter Atomic Decomposition of Chirplets," *IEEE Trans. Signal Processing*, Vol. 47, March 1999, pp. 731–745.

[14] Wigner, E. P., "On the Quantum Correction for Thermodynamic Equilibrium," *Phys. Rev.*, Vol. 40, 1932, pp. 749.

[15] Ville, J., "Theorie et Applications de la Notion de Signal Analytique," *Cables et Transmission*, Vol. 2, 1948, pp. 61–74.

[16] Page, C. H., "Instantaneous Power Spectra," *J. Appl. Phys.*, Vol. 23, 1952, pp. 103–106.

[17] Margenau, H., and R. N. Hill, "Correlation Between Measurements in Quantum Theory," *Prog. Theoret. Phys.*, Vol. 26, 1961, pp. 722–738.

[18] Rihaczek, A. W., "Signal Energy Distribution in Time and Frequency," *IEEE Trans. Inform. Theory*, Vol. IT-14, 1968, pp. 369–374.

[19] Cohen, L., "Generalized Phase-Space Distribution Functions," *J. Math. Phys.*, Vol. 7, 1966, pp. 781–806.

[20] Choi, H., and W. J. Williams, "Improved Time-Frequency Representation of Multi-component Signals Using Exponential Kernels," *IEEE Trans. Acoustics, Speech, Signal Processing*, Vol. ASSP-37, June 1989, pp. 862–871.

[21]   Zhao, Y., L. E. Atlas, and R. J. Marks, "The Use of Cone-Shaped Kernels for Generalized Time-Frequency Representations of Nonstationary Signals," *IEEE Trans. Acoustics, Speech, Signal Processing*, Vol. ASSP-38, July 1990, pp. 1084–1091.

[22]   Qian, S., and D. Chen, "Decomposition of the Wigner-Ville Distribution and Time-Frequency Distribution Series," *IEEE Trans. Signal Processing*, Vol. SP-42, October 1994, pp. 2836–2842.